Title

Boundary Layer Diabatic Processes, the Virtual Effect, and Convective Self-Aggregation

Journal

Journal of Advances in Modeling Earth Systems, 10(9)

ISSN

1942-2466

Author

Yang, Da

Publication Date

2018-09-01

DOI

10.1029/2017ms001261

Peer reviewed

Journal of Advances in Modeling Earth Systems

RESEARCH ARTICLE
10.1029/2017MS001261

Boundary Layer Diabatic Processes, the Virtual Effect, and Convective Self-Aggregation

Da Yang[1,2]

[1]University of California, Davis, CA, USA, [2]Lawrence Berkeley National Laboratory, Berkeley, CA, USA

Key Points:
- The available potential energy production for self-aggregation is mainly in the boundary layer
- Boundary layer diabatic processes are key to convective self-aggregation
- The enhanced virtual effect could lead to self-aggregation in the absence of radiative feedbacks

Correspondence to:
D. Yang,
dayang@ucdavis.edu

Citation:
Yang, D. (2018). Boundary layer diabatic processes, the virtual effect, and convective self-aggregation. *Journal of Advances in Modeling Earth Systems*, *10*, 2163–2176. https://doi.org/10.1029/2017MS001261

Received 17 DEC 2017
Accepted 7 JUN 2018
Accepted article online 20 JUN 2018
Published online 6 SEP 2018

Abstract The atmosphere can self-organize into long-lasting large-scale overturning circulations over an ocean surface with uniform temperature. This phenomenon is referred to as convective self-aggregation and has been argued to be important for tropical weather and climate systems. Here we present a boundary layer centric framework based on the available potential energy budget of convective self-aggregation. We show that boundary layer diabatic processes dominate the available potential energy production and are, therefore, essential to convective self-aggregation. We further show that the enhanced virtual effect of water vapor can lead to convective self-aggregation.

1. Introduction

It would be intuitive if convection were homogeneously distributed in nonrotating radiative-convective equilibrium (RCE). Held et al. (1993), however, showed that convective storms could aggregate into a single cluster surrounded by an area with weak subsidence and very dry conditions. This phenomenon is now referred to as convective self-aggregation and has been extensively studied using a hierarchy of numerical models across a wide range of climates (Abbot, 2014; Arnold & Randall, 2015; Bretherton et al., 2005; Coppin & Bony, 2015; Holloway & Woolnough, 2016; Jeevanjee & Romps, 2013; Muller & Bony, 2015; Muller & Held, 2012; Wing & Cronin, 2015; Yang, 2018).

Understanding convective self-aggregation may advance our understanding of the Madden-Julian ocillation (MJO), a long-term mystery of tropical meteorology. MJO-like signals have been successfully simulated over uniform boundary conditions using shallow water models (Yang & Ingersoll, 2013, 2014) and the superparameterized Community Atmosphere Model (Arnold & Randall, 2015; Pritchard & Yang, 2016). Arnold and Randall (2015) further showed that the feedbacks responsible for maintaining the MJO might be the same as those responsible for convective self-aggregation. It is therefore suggested that the MJO could be a form of convective self-aggregation over an equatorial beta plane (Bretherton et al., 2005).

Previous studies have suggested that radiative feedbacks in the free troposphere (FT) are important to convective self-aggregation (Bretherton et al., 2005; Emanuel et al., 2014; Muller & Held, 2012). A key recipe in the previous framework is the weak buoyancy gradient (WBG) approximation, which was first discussed by Charney (1963), then further developed by Sobel et al. (2001) and others, and recently evaluated in 2-D self-aggregation simulations by Yang (2018). The direct effect of WBG suggests that anomalous radiative cooling generates sinking motion, which dries the atmosphere. Drier atmosphere then promotes radiative cooling, which further dries the atmosphere column and closes the feedback loop (Emanuel et al., 2014).

Although the FT framework has provided much insight on the development of self-aggregation, there is a growing evidence suggesting that boundary layer (BL) processes are important to self-aggregation (Muller & Bony, 2015; Naumann et al., 2017). For example, evaporation of raindrops in the BL has been found to inhibit self-aggregation (Jeevanjee & Romps, 2013; Muller & Bony, 2015), which may not be explained by the prevailing FT centric framework.

This paper presents a BL centric framework. This framework is built up on an indirect effect of the WBG approximation: BL diabatic processes dominate the production of available potential energy (APE) as there is little buoyancy perturbation in FT. Continuing production of APE is required to develop and to maintain self-aggregated circulations. This framework, therefore, predicts that BL diabatic processes are key to convective self-aggregation. This framework further suggests that the enhanced virtual effect could favor self-aggregation, and evaporation of raindrops inhibits self-aggregation, according to their effects on APE

production. This study emphasizes the self-aggregated circulation and the associated APE production, complementing the view obtained from analyzing the FT thermodynamic feedbacks and the associated moist static energy budget (Bretherton et al., 2005; Emanuel et al., 2014).

2. Model Setup

We perform self-aggregation simulations using the System for Atmosphere Modeling (SAM version 6.10.8; Khairoutdinov & Randall, 2003). SAM is an anelastic model. The radiation scheme is identical to that of the National Center for Atmospheric Research Community Atmosphere Model version 3 (Collins et al., 2006). The incoming solar radiation is fixed at 413.9 W/m^2 to match the annual mean insolation on the equator (Cronin, 2014), and the diurnal cycle is turned off. The microphysics is the SAM one-moment parameterization. The domain mean horizontal wind is nudged to 0 at all vertical levels. In Appendix, we show that nudging horizontal winds does not affect the overall result.

In this paper, we present results from twenty-six 120-day 2-D SAM simulations. In each simulation, the horizontal domain size is 2,048 km, and the model top is at 34.8 km. The horizontal resolution is 2 km. The vertical resolution is 50 m for the lowest 1 km and increases to 600 m above 3 km. A sponge layer is employed for the upper 6 km of the model domain. The model is coupled to an ocean surface with a fixed, uniform sea surface temperature of 300 K. All simulations are initialized with the same RCE profile. To test the sensitivity to initial conditions, we have also performed simulations initialized with their respective RCE profiles, and the qualitative results are the same.

We switch on and off some physical processes to test the their causal relation with convective self-aggregation. We perform these experiments for the FT and BL separately, and this allows us to test if BL is the key. In this paper, we separate FT and BL at the altitude of 2 km, where the horizontal pressure and buoyancy gradients are small at steady state (Yang, 2018). We also explore the sensitivity of choosing a different BL top in Appendix.

3. The APE Framework

The APE is the energy reservoir for dynamics, so its production is key to generate instability and to maintain long-lasting overturn circulations. This concept has been used in studying large-scale tropical waves: APE consumption leads to decaying waves (Emanuel et al., 1994), and APE production leads to amplifying waves (Kuang, 2008a, 2008b). Here we calculate the APE budget for convective self-aggregation in a 2-D anelastic atmosphere. This analysis will help us understand what physical processes generate APE and amplify circulations. In the following calculation, APE should be considered as the eddy APE, which measures the APE around the reference state. The numerical value of the eddy APE measures the strength of self-aggregation but could not be used to determine if the reference state is at its minimum potential energy state.

3.1. Derivation

In an anelastic atmosphere, the APE is defined as

$$APE = \frac{1}{2}\int_0^z \rho_0 \mathrm{d}z \frac{\overline{b^2}}{N^2}, \tag{1}$$

where $\rho_0 = \rho_0(z)$ is the reference density, b is buoyancy, $N^2 = N^2(z)$ is the Brunt Vaisala frequency, and the overbar denotes horizontal average. This definition of APE differs from its Boussinesq version by including $\rho_0 = \rho_0(z)$ (Vallis, 2017). The evolution of APE can be derived by using the buoyancy equation

$$\partial_t b + u\partial_x b + wN^2 = S_b, \tag{2}$$

where (u, w) are horizontal and vertical wind speeds, respectively, and S_b represents buoyancy sources. Because we are only interested in the APE associated with self-aggregation circulations, which varies slowly, we would like to filter out high-frequency, small-scale waves. If we denote $\tilde{A}$ as the slow component of A, the buoyancy equation for the slow component is

$$\partial_t \tilde{b} + \widetilde{u\partial_x b} + \tilde{w}N^2 = \tilde{S}_b. \tag{3}$$

The APE budget of the slow component (convective self-aggregation) is given by

$$\overbrace{\frac{1}{2}\int_0^z \frac{\rho_0 dz'}{N^2}\partial_t \widetilde{\overline{b}^2}}^{\partial_t \widetilde{\mathrm{APE}}} = \overbrace{\int_0^z \frac{\rho_0 dz'}{N^2}\widetilde{\overline{b}}\widetilde{\overline{S}_b}}^{\text{Production}} - \underbrace{\int_0^z \frac{\rho_0 dz'}{N^2}\widetilde{\overline{bu}\partial_x b}}_{\text{Advection}} - \underbrace{\int_0^z \rho_0 dz' \widetilde{\overline{b}}\widetilde{\overline{w}}}_{\text{Conversion}}. \quad (4)$$

Equation (4) is the key equation of our diagnostic framework and will be used to diagnose cloud-resolving model (CRM) simulations.

The production of APE is the key: Positive values correspond to amplifying effects, and negative values correspond to decaying effects (Emanuel et al., 1994; Kuang, 2008a, 2008b). This suggests that powering the circulation relies on positive correlations between buoyancy sources and buoyancy anomalies when the atmosphere is stably stratified. More details on calculating the APE production is in Appendix A.

3.2. An Indirect Effect of WBG

In a slowly or nonrotating atmosphere, there is limited APE production in the FT for large-scale long-lasting circulations. This is because the APE production requires buoyancy anomalies, which are effectively smoothed out by gravity waves in the FT (WBG; Charney, 1963; Sobel et al., 2001; Yang, 2018). This then suggests that BL processes dominate the APE production if FT is in the WBG regime (H1).

According to this indirect effect of WBG (H1), we hypothesize that BL diabatic processes are the key to large-scale long-lasting circulations, including convective self-aggregation (H2).

3.3. The Virtual Effect, Buoyancy, and Its Sources

Buoyancy in a moist atmosphere is, to a good approximation, given by

$$b = g\frac{\theta_v'}{\bar{\theta}_v} = g\left(\frac{\theta'}{\bar{\theta}} + \frac{\epsilon q'}{1+\epsilon\bar{q}}\right), \quad (5)$$

where g is the gravitational acceleration (m/s^2), θ_v is the virtual potential temperature (K), θ is the potential temperature (K), q is the specific humidity (kg/kg), and $\epsilon = M_{\mathrm{Air}}/M_{\mathrm{H_2O}} - 1 = 0.61$. The dependence on q is because the molar mass of water is lighter than that of dry air. This suggests that a moist parcel would be lighter than a dry parcel given the same temperature, pressure, and volume, which is referred to as the virtual effect of water vapor. According to (5), buoyancy sources should include both heat sources (S_θ) and moisture sources (S_q), and they are related by

$$S_b = g\frac{S_\theta}{\bar{\theta}} + g\frac{\epsilon S_q}{1+\epsilon\bar{q}}. \quad (6)$$

This suggests that warming and moistening are both buoyancy sources, and cooling and drying are buoyancy sinks. Therefore, varying the strength of the virtual effect could change the APE production and thereby alter the behavior of convective self-aggregation (H3).

We consider four different diabatic processes, including radiation, surface fluxes, evaporation, and condensation. Radiation only contributes to S_θ and is an external process. The other processes contribute to both S_θ and S_q. Surface latent and sensible heat fluxes are also external processes to the atmosphere. At the global scale, their sum is constrained by the surface energy balance. However, there are no such constraints on local transient surface fluxes, which are most relevant to convective self-aggregation. Evaporation and condensation are internal processes and both have opposing effects on buoyancy. Evaporation increases moisture ($S_q > 0$; buoyancy source) but cools the atmosphere (S_θ<0; buoyancy sink). Condensation does the opposite. Which effect is dominant? During the phase change, sensible energy is converted to latent energy: $LS_q = -c_p S_\theta$, where L is the latent heat of water vapor (J/kg). This leads to

$$\frac{S_\theta/\bar{\theta}}{\epsilon S_q/(1+\epsilon\bar{q})} \sim \frac{(1+\epsilon\bar{q})S_\theta}{\epsilon\bar{\theta}S_q} = -\frac{(1+\epsilon\bar{q})}{\epsilon}\frac{L}{c_p\bar{\theta}} \approx -13.8. \quad (7)$$

This scaling result suggests that convective heating and evaporative cooling dominate over the associated drying and moistening effects. However, this relation would be subject to change if ϵ is varied.

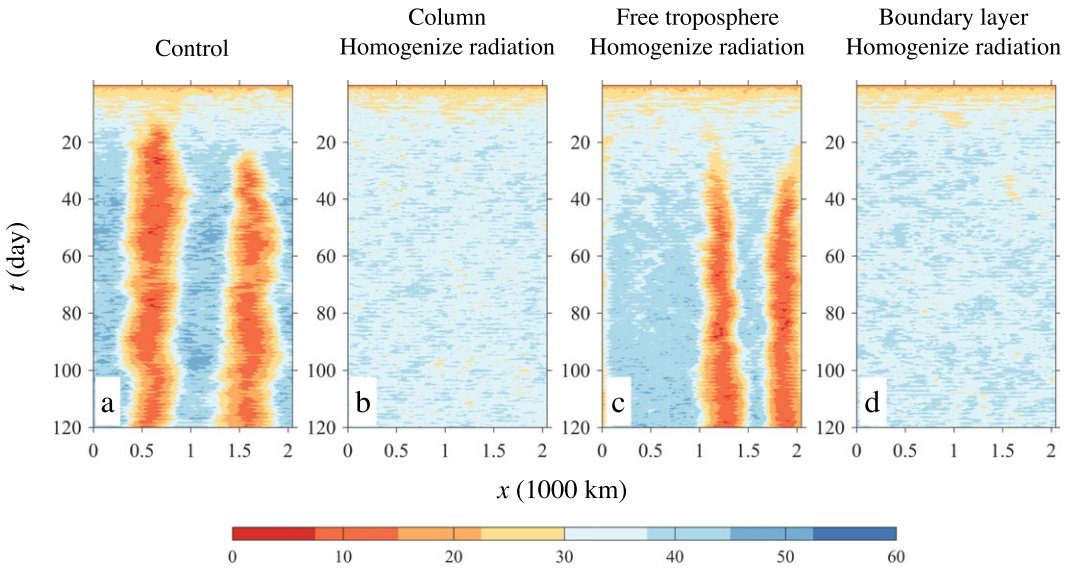

Figure 1. Examine the role of radiation. Hovmöller diagrams of precipitable water (mm) in the control simulation (a) and in simulations with horizontally homogenized radiative cooling rates for the entire column (b), for the free troposphere (c), and for the boundary layer (d).

3.4. Diagnostic Results

We use (4) to calculate the APE budget in two SAM simulations: a control simulation (with self-aggregation, Figure 1a) and a simulation with horizontally homogenized radiative cooling rates (no self-aggregation, Figure 1b). We will first discuss the control simulation in detail and then compare it with the homogenized-radiation simulation.

Figure 1a shows the Hovmöller diagram of precipitable water (PW) from our control simulation. Two large-scale convective envelopes self-emerged over uniform sea surface temperature. Such multiple aggregates have been shown in previous studies, and a quantitative theory was developed to explain what sets the spatial scale of convective self-aggregation (Yang, 2018).

Figure 2 illustrates the evolution of the large-scale circulation associated with convective self-aggregation for three time periods: day 5–20 (left), day 15–30 (middle), and day 50–80 (right). The first two periods are in the developing phase, and the last time period represents the steady state. During period 1, moisture starts to aggregate (Figure 1a), and the associated large-scale circulation starts to develop: Horizontal wind divergence and a high pressure center are collocated with the dry center. During period 2, the wind and pressure anomalies are enhanced, together with the moisture anomaly. Because p' is negligible at the BL top compared with p' in the BL, the enhanced high pressure anomaly is associated with negative buoyancy anomalies (Yang, 2018). By comparing periods 2 and 3, we find that the dry patch-associated circulation and pressure anomalies are well established in period 2, but the moist patch-associated circulation and pressure anomalies continue to develop. This asymmetric development was also noticed in previous studies focusing on the moisture organization (Bretherton et al., 2005; Muller & Held, 2012) and is likely due to the stronger anomalous diabatic processes in the dry area.

Figure 3a shows evolution of APE of the large-scale circulation, calculated using 15-day running-averaged buoyancy according to (1). The 15-day running average captures convective self-aggregation very well (Figure 2), and the overall trend of the APE is robust to different choices of window width (e.g., 10 or 20 days). The APE first increases with time till day 50 and then reaches a statistically steady state. This result is consistent with Figure 3b, plotting the variance of PW in the same simulation. It has been shown that the variance of PW significantly increases in the aggregated simulations (Arnold & Randall, 2015; Bretherton et al., 2005). This consistency then suggests that the evolution of APE is able to characterize the behavior of the circulation. Therefore, diagnosing that the APE budget would help to understand what leads to increase in APE and strengthening in circulation.

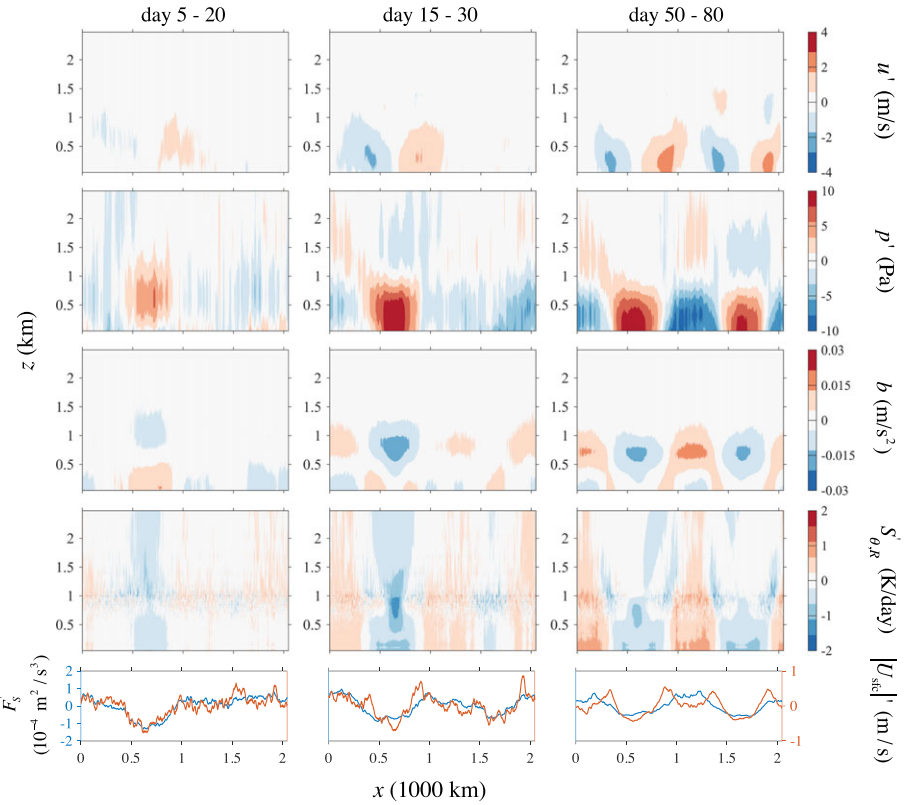

Figure 2. Diagnostics for the control simulation in Figure 1a. The top to bottom rows correspond to time-averaged u' (wind anomalies), p' (pressure anomalies), b (buoyancy), $S'_{\theta,R}$ (radiative cooling rate anomaly), F'_S (surface buoyancy flux anomalies) , and $|U_{sfc}|'$ (anomalies of surface-wind amplitudes) , respectively. The left to right rows are for three time periods: day 5–20, day 15–30, and day 50–80.

Figure 4a shows the APE budget associated with convective self-aggregation in the control simulation. The total APE production is mainly balanced by its conversion to kinetic energy, and their small difference leads to slowly growing circulations. The nonlinear advection can be negligible throughout the entire simulation period, suggesting that dynamics are linear to the leading order.

The diabatic APE production dictates the energy conversion rate and powers the circulation. Here we discuss three diabatic processes that generates APE: convection, radiation, and surface buoyancy fluxes. The first two processes are dominant. Their amplitudes increase with time during the first 50 days and then start to oscillate around their reference values, reaching statistical equilibrium. This result suggests that the development of convective self-aggregation could be associated with enhanced APE production mainly due to convective heating and radiative cooling. The APE production due to surface fluxes is small except for the first 20 days.

Figure 4b shows that the total diabatic production of $\widetilde{APE}$ in the BL is about 4 times larger than that in the FT (black lines in Figure 4b). This is an indirect effect of gravity waves and WBG in the FT (Charney & Eliassen, 1964; Sobel et al., 2001; Yang, 2018). The production of APE relies on the correlation between diabatic processes and buoyancy anomalies. As there is almost no buoyancy anomalies in the FT, the APE production is limited. This result validates our H1 and also motivates H2.

Why do convection, radiation, and surface fluxes generate APE?

1. Convection occurs in the moist patch and heats the buoyant part of the BL. The cloud base is below the BL top (2 km), above which buoyancy and pressure perturbations are small. Therefore, convective heating is an effective buoyancy source in the BL and can generate APE.
2. Radiative cooling is more efficient over the dry patch (the fourth row $S'_{\theta,R}$ in Figure 2). In period 1, radiative cooling and buoyancy anomalies are positively correlated in the upper part of the BL, but they are negatively correlated in the lower part of the BL (Figure 2). The overall effect is negative (Figures 4a and 4b), suggesting that radiation is not responsible for the development of convective self-aggregation during

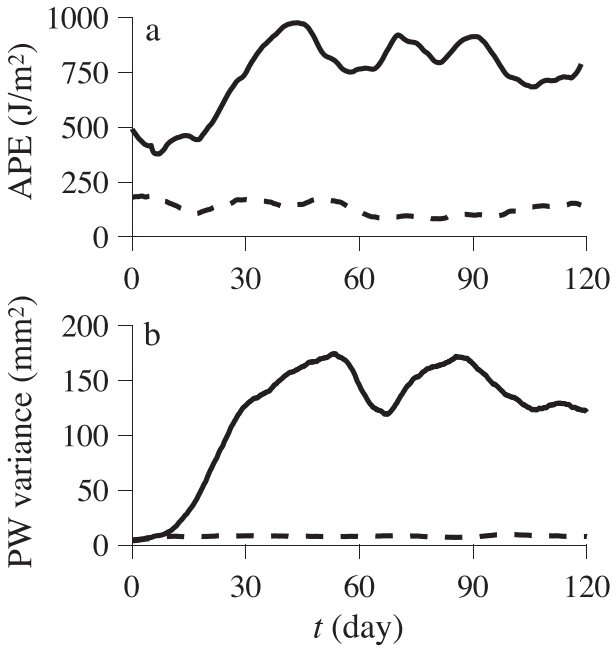

Figure 3. Evolution of (a) APE and (b) PW variance associated with long-lasting circulations. Solid line represents the control simulation, and the dashed line represents the simulation with homogenized radiation for the entire column. APE = available potential energy; PW = precipitable water.

the first 20 days. In periods 2 and 3, radiative cooling is positively correlated with buoyancy anomalies in the entire BL (Figure 2), so its APE production is positive, contributing to the growth of self-aggregation. Radiative feedbacks then favors self-aggregation during most of the simulation period, which is consistent with previous mechanism-denial experiment results (Bretherton et al., 2005; Muller & Bony, 2015).

3. The surface buoyancy flux is only effective in period 1, when it is negatively correlated with surface buoyancy anomalies (the fifth row in Figure 2). This negative correlation would lead to negative APE production if N^2 is positive at surface. However, N^2 is negative within the surface layer as buoyancy flux is down gradient from surface to atmospheric BL. This is a classic result (Garratt, 1994) and is also evident in our simulations (Figure B1). This negative correlation can then generate APE. In periods 2 and 3, the spatial pattern of surface fluxes remains the same, but buoyancy anomalies at surface become weaker (Figure 2), leading to smaller APE production.

   Previous studies have explored the role of surface fluxes (Bretherton et al., 2005; Muller & Held, 2012) in the context of entropy or moist static energy. Here we emphasize the role of buoyancy fluxes that depend on the virtual effect of water vapor. The virtual effect helps amplify $S_{q,S}$ according to equation (6). Local transient surface fluxes are not constrained by surface energy balance. The enhanced virtual effect, therefore, leads to enhanced surface buoyancy flux and favors convective self-aggregation if there is no dramatic change of the Bowen ratio.

Evaporation of raindrops is active in this simulation and its effect is to inhibit self-aggregation. Evaporation occurs in the moist patch, where there is positive buoyancy anomaly. This effect, therefore, reduces APE and inhibits convective self-aggregation. We will present mechanism-denial experiments and scaling arguments to test this hypothesis.

We also calculate APE and its budget in a simulation without self-aggregation (Figures 1b, 3, and (4)). APE remains at a modest level, consistent with the evolution of PW variance, and the production of APE is an order of magnitude smaller than that in the control simulation. This difference may suggest that convection only self-aggregates when there is sufficient APE production, which is dominated by BL diabatic processes.

4. Mechanism-Denial Experiments

In this section, we show results from mechanism-denial CRM simulations to understand the causal effects of individual diabatic processes and to test H2 and H3.

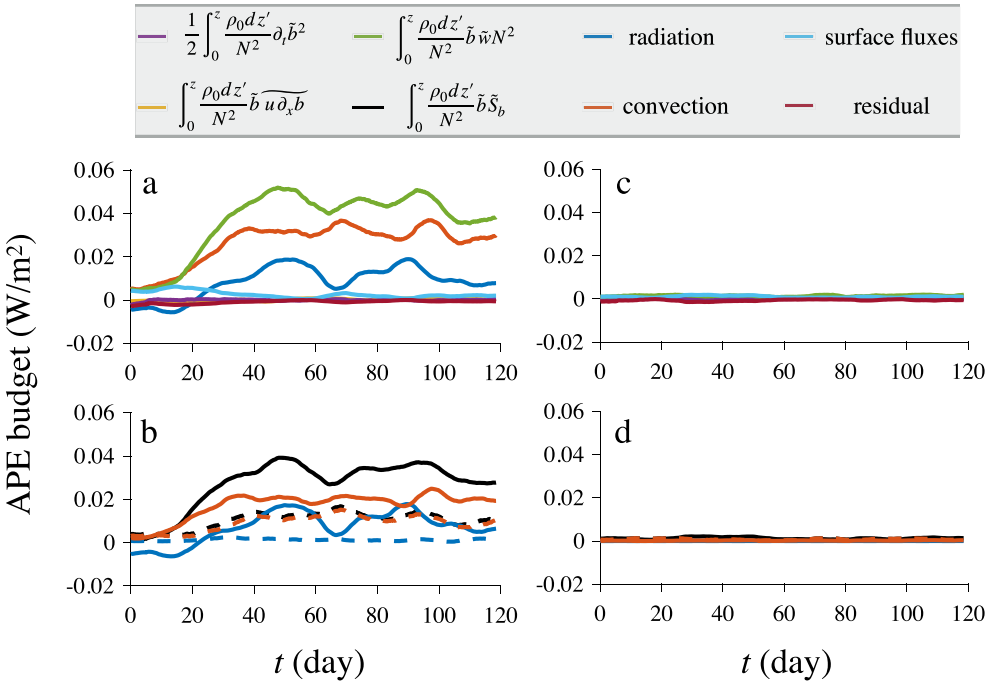

Figure 4. The APE budget for (a, b) the control simulation and (c, d) the simulation with homogenized radiation for the entire column. Panels (a) and (c) are the APE budget for the entire column, and panels (b) and (d) are the APE budget for boundary layer, the lowest 2 km. In (b) and (d), solid lines represent boundary layer contributions, and dashed lines represent free troposphere contributions. APE = available potential energy.

4.1. Radiation

Figure 1 shows that inhomogeneous radiative cooling in the BL helps convection self-aggregate. Figure 1b shows results of a mechanism-denial experiment, in which radiative cooling rate is homogenized horizontally throughout the entire column. Convection does not self-aggregate in the 120-day simulation period. This result suggests that radiative feedbacks can help develop and maintain convective self-aggregation.

The APE analysis of our control simulation shows that radiation in general generates APE except for the first 20 days (solid line in Figure (4)). One may, therefore, expect that convection would first aggregate and then disaggregate in this mechanism-denial experiment. Convection, however, does not aggregate at all (Figure 1b). This result would seem to contradict our diagnostic analysis if the APE production of all other components remain unchanged, which is, however, unlikely in such a highly nonlinear system. Our APE analysis indeed agrees with this mechanism-denial experiment, suggesting that the overall effect of radiative feedbacks favors self-aggregation in the control simulation.

We then separately test the role of radiative feedback in the FT and that in the BL. We find that convection can still self-aggregate when only homogenizing radiative cooling in the FT (Figure 1c), but convection cannot self-aggregate during the 120-day simulation period if we only homogenize radiative cooling in the BL (Figure 1d). This set of experiments, therefore, suggests that interactive radiative cooling in the BL is important to convective self-aggregation. This result supports our hypothesis (H2) and APE budget analysis (Figure 4) and is also consistent with Naumann et al. (2017), who suggested that differential radiative cooling in the BL is able to drive circulations.

For the rest of this paper, we keep radiative cooling homogenized for the entire column and investigate the role of other diabatic processes.

4.2. The Virtual Effect and Surface Buoyancy Flux

In this set of experiments, we enhance the virtual effect by increasing ϵ in SAM. Figure 5 shows that enhancing the virtual effect either for the entire column (first row) or for the BL (third row) can lead to convective self-aggregation even without radiative feedbacks. However, enhancing the virtual effect only for the FT (second row) does not lead to convective self-aggregation during the 120-day simulation period. These results

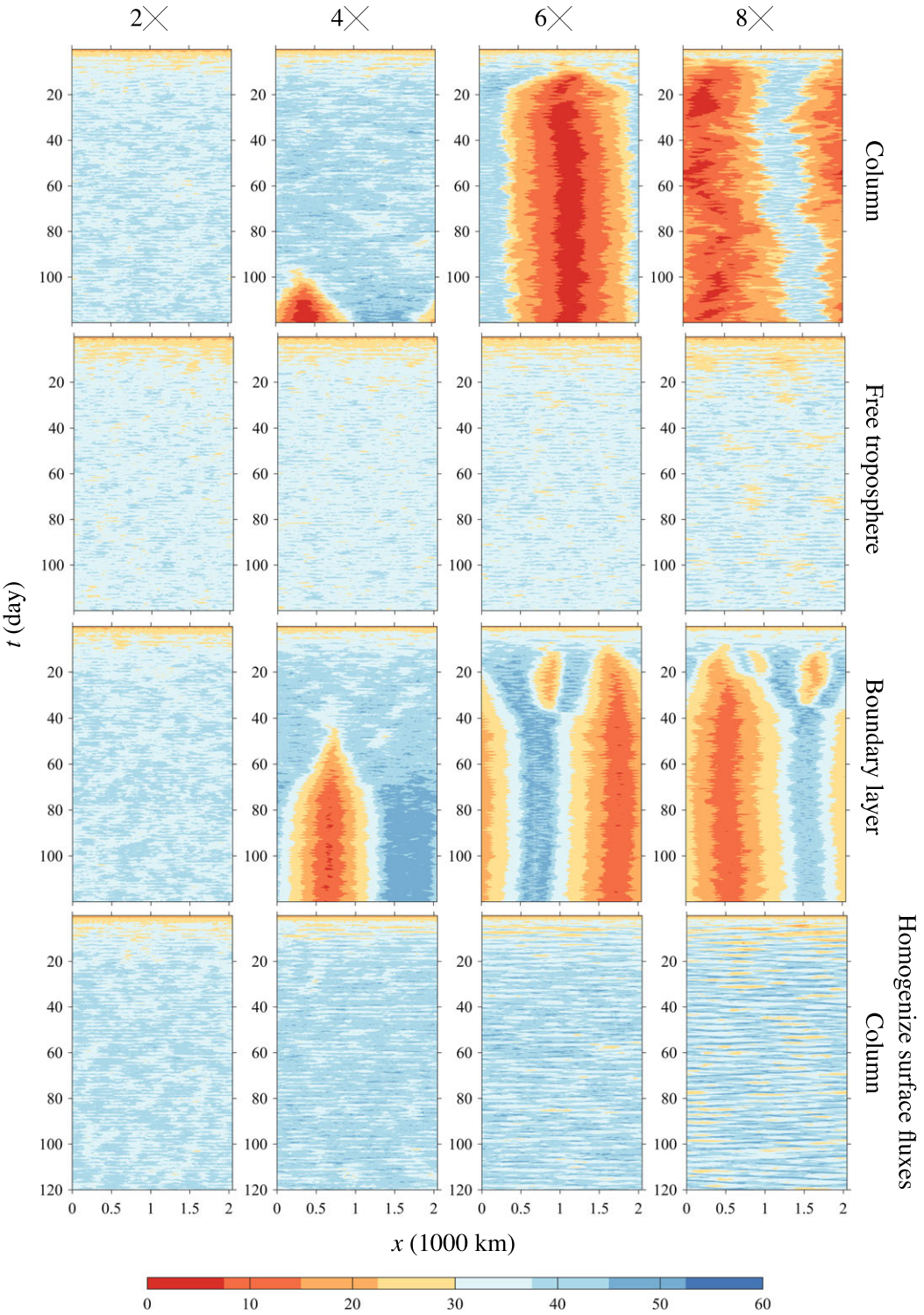

Figure 5. Examine the role of the virtual effect and surface buoyancy fluxes. All figures show Hovmöller diagrams of precipitable water (mm) in cloud-resolving simulations with horizontally homogenized radiative cooling. The virtual effect is enhanced gradually from 2 times ($\epsilon = 2 \times 0.61 = 1.22$, the left column) to 8 times ($\epsilon = 8 \times 0.61 = 4.88$, the right column). In the first row, the virtual effect is enhanced for the entire column. In the second row, the virtual effect is enhanced only for the free troposphere. In the third row, the virtual effect is enhanced only for the BL. In the last row, the virtual effect is enhanced for the entire column, and the surface buoyancy flux is homogenized.

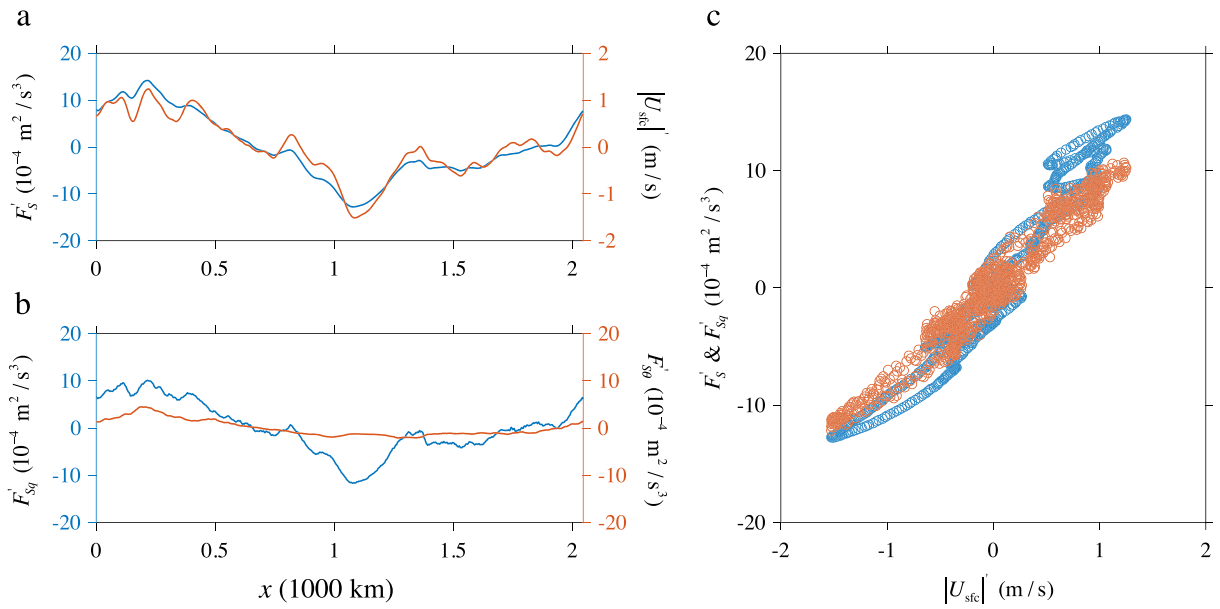

Figure 6. The surface buoyancy flux and its relation to the surface wind in the 6× virtual effect simulation. (a) Left: the anomaly of surface buoyancy flux F_s'. Right: the anomaly of the amplitude of surface wind. (b) Left: the anomaly of surface buoyancy flux due to latent heat flux F_{sq}'. Right: the anomaly of surface buoyancy flux due to sensible heat flux $F_{s\theta}'$. (c) The anomaly of surface buoyancy fluxes versus the anomaly of the amplitude of the surface wind. All results are averaged over day 5–20 of the simulation.

again highlight the importance of BL processes (H1 and H2) and also supports H3. Convection, however, does not self-aggregate even with enhanced virtual effect when we homogenize the surface buoyancy flux (the bottom row of Figure 5). These results suggest that the enhanced virtual effect could enhance surface buoyancy fluxes, leading to self-aggregation.

Here we use the 6× virtual effect simulation to illustrate the self-aggregation mechanism. Figure 6 shows that the amplitude of anomalous surface buoyancy fluxes (F_s') is much larger than that in the control simulation (Figure 2) and that the spatial variation is still in phase with the aggregation pattern (the same phase relation as in the control simulations). This suggests that surface buoyancy fluxes are more effective in amplifying circulation anomalies, leading to convective self-aggregation in the absence of radiative feedbacks.

In this simulation, F_s' is dominated by the moisture contribution F_{sq}' (Figures 6a and 6b), which has increased significantly from the control simulation (Figure 2). This increase mainly results from the 6× enhancement of the virtual effect. The surface buoyancy flux due to temperature $F_{s\theta}'$ almost maintains its amplitude from the control experiment, so $F_{s\theta}'$ is not responsible for the amplification of F_s'.

The spatial pattern of F_s' and F_{sq}' is associated with $|U_{sfc}|'$, which is enhanced in the moist region likely due to gustiness (Figure 6a). Figure 6c plots F_s' and F_{sq}' against $|U_{sfc}|'$. There is a strong linear relation between surface wind and buoyancy anomalies: The correlation coefficients are 0.96 and 0.86 for (F_s', $|U_{sfc}|'$) and (F_{sq}', $|U_{sfc}|'$), respectively. This suggests that $|U_{sfc}|'$ is the dominant factor determining the spatial variation of F_s' and F_{sq}' and their phase relation to the aggregated circulation.

We test the robustness of these results by perturbing the model setup. We have performed a simulation without nudging the domain mean horizontal wind (Figure B3). Convection still aggregates, suggesting that nudging horizontal winds has limited effects on the proposed feedback. In SAM, there is a minimum surface wind threshold in formulating surface fluxes. The threshold is set as 1 m/s in all of the presented simulations. We have also performed simulations with 0.1 m/s surface wind threshold (not shown) and find that our results are robust over this one order of magnitude change of the surface wind threshold. For example, convection still self-aggregates with 6× virtual effect due to amplified F_{sq}'.

For the rest of this paper, we horizontally homogenize radiative cooling and surface buoyancy fluxes to focus on the role of other diabatic processes.

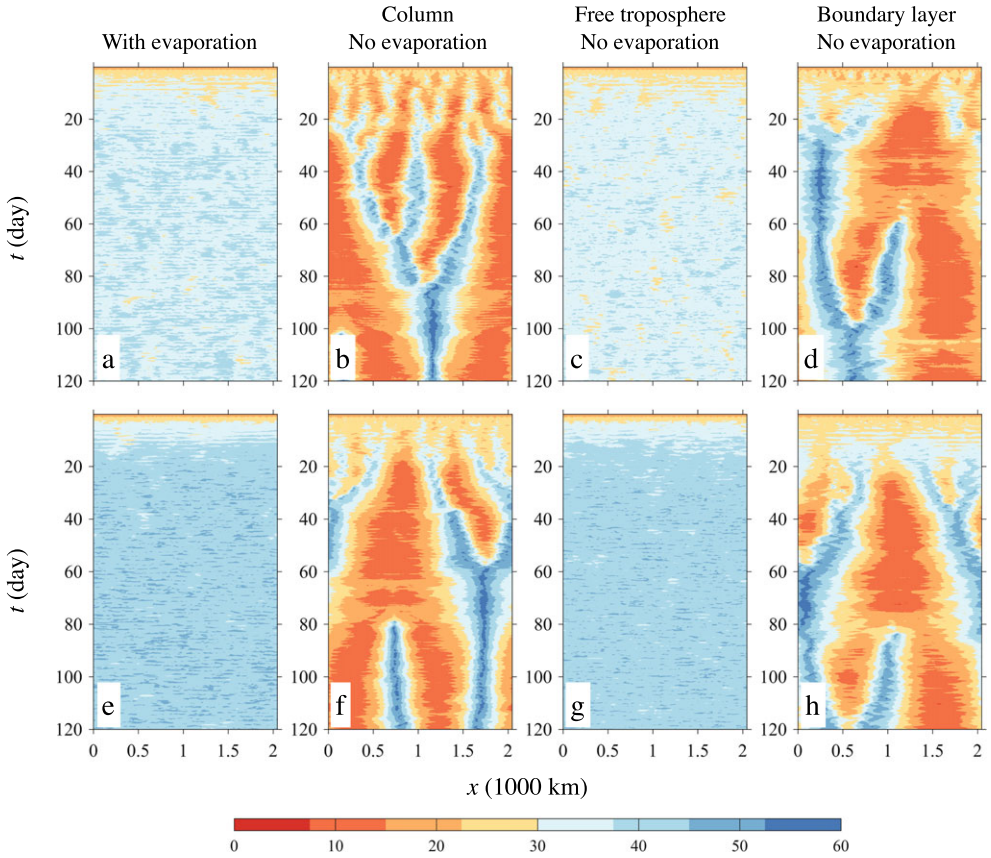

Figure 7. Examine the role of evaporation of raindrops. Hovmöller diagrams of precipitable water (mm) in the simulation with evaporation (a, e), without evaporation in the entire column (b, f), without evaporation in the free troposphere (c, g), without evaporation in the boundary layer (d, h). All simulations are performed with horizontally homogenized radiative cooling rates and surface fluxes. The upper-panel simulations use the default microphysics scheme; the lower-panel simulations use the same microphysics scheme without the accretion process.

4.3. Evaporation of Raindrops

Jeevanjee and Romps (2013) switched off evaporation of raindrops in the BL and discovered that *cold pools* could inhibit convective self-aggregation. Muller and Bony (2015) turned off cold pools using the same method and found that convection can still aggregate even without radiative feedbacks, which further confirmed the effect of switching off evaporation in self-aggregation. Here we show that it is not the cold pool of air but the evaporative cooling that inhibits convective self-aggregation. In this set of experiments, we switch on and off evaporation of raindrops following Jeevanjee and Romps (2013) and Muller and Bony (2015). Because inhibiting raindrop evaporation may promote anomalous rain formation through the accretion process, we perform a set of sensitivity experiments by switching off the accretion process. These two sets of simulations are two end members in rain formation. Our sensitivity experiments can, therefore, confirm the robustness of the results.

Convection does not self-aggregate if evaporation is active in the entire column (Figure 7a) or only in the BL (Figure 7c). This suggests that evaporation in the FT has limited effects on convective self-aggregation. We also find that convection, however, starts to aggregate when we switch off evaporation either in the entire column or only in the BL (Figures 7b and 7d). This contrast suggests that evaporation in the BL inhibits convective self-aggregation. Our no-accretion experiments show similar results, supporting our hypothesis (Figure 7e–7h).

Jeevanjee and Romps (2013) suggested that cold pools can inhibit convective self-aggregation by effectively homogenizing BL properties between moist and dry patches. However, scale analyses of our simulations suggest the opposite—cold pools should not be effective. The homogenizing effect should only operate over the scale of cold pools. Gentine et al. (2016) showed that the horizontal scale of cold pools is of O (20–30 km)

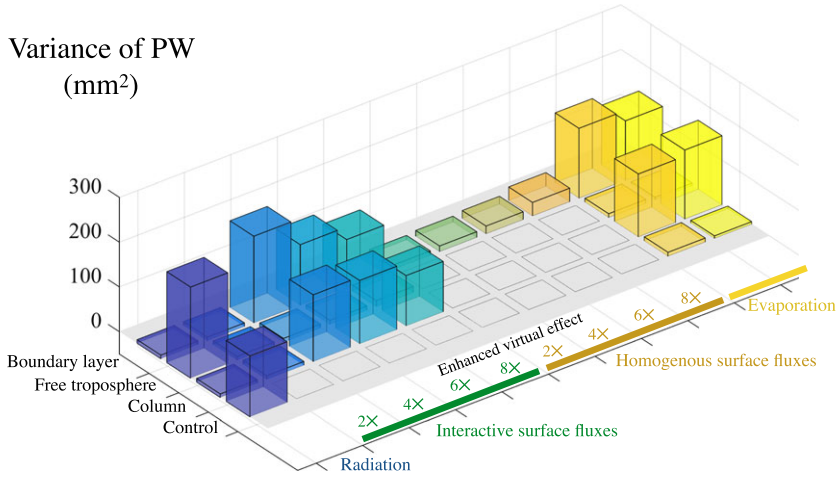

Figure 8. Summary of all experiments. The horizontal axes label individual experiments: One axis labels the physical process that we switch on and off to study its role on self-aggregation, and the other axis labels where we switch on or off the physical process. The *control* row indicates the simulations that we keep the corresponding process unchanged. The vertical axis labels the amplitude of PW variation in the last 40 days of corresponding simulations. High-variance simulations are the ones that have convective self-aggregation. The variance of PW in the *column* and *boundary layer* rows are comparable, suggesting that diabatic processes in the boundary are key to convective self-aggregation.

using the same CRM (SAM) in a variety of setups (see their Figures 3 and 4). However, the horizontal scale of aggregation in our simulations is of O (1,000 km), almost two orders of magnitude larger than the effective scale of cold pools. Individual cold pools, therefore, may not effectively homogenize BL properties. Evaporative cooling in the BL reduces the buoyancy anomaly in the moist patch and can, therefore, inhibit convective self-aggregation.

What leads to convective self-aggregation in the absence of interactive radiation and surface fluxes, and evaporation of raindrops? According to our framework, we speculate that it is the remaining diabatic processes in the BL that lead to self-aggregation. Convective heating and turbulent entrainment are the two distinct and yet related candidates. The role of convective heating is already evident in our control simulation (orange lines in Figures 4a and 4b): It dominates the APE production. When evaporative cooling is switched off, more net convective heating is realized, which could produce APE more effectively, leading to self-aggregation by itself. This idea is consistent with Yang and Ingersoll (2013, 2014) and might be also consistent with the broadly defined conditional instability of the second kind (Charney & Eliassen, 1964; Wu, 2003). Entrainment is another process that could lead to self-aggregation as suggested by Tompkins and Semie (2017) and Tompkins (2001). Identifying which process is at work in this simulation is a next step toward better understanding convective self-aggregation.

Figure 8 plots the variance of PW in the last 20 days of all simulations and highlights the BL processes. All aggregated simulations have high variance of PW, and nonaggregated simulations have low variance of PW. The *column* and *boundary layer* experiments always have comparable variance of PW, but the column and *free troposphere* experiments always have opposite results. We therefore conclude that the BL diabatic processes are key to convective self-aggregation (H1 and H2).

5. Conclusion and Discussions

This paper presents a BL framework to understand the initiation of convective self-aggregation. The initiation is a coupled process: It is related to the growth of both dynamic and thermodynamic perturbations in the BL, including horizontal wind, buoyancy, and pressure perturbations (Figure 2). The growth of wind anomalies requires horizontal pressure gradient. Assuming weak pressure gradient above the BL, the buoyancy gradient within the BL is necessary to establish a BL pressure gradient (Yang, 2018). We then use our APE framework and CRM simulations to demonstrate that BL diabatic processes are necessary to amplify density and pressure perturbations and are thereby essential for the initiation of convective self-aggregation. This new framework successfully predicts the role of the virtual effect and could help unify the current understanding of convective self-aggregation.

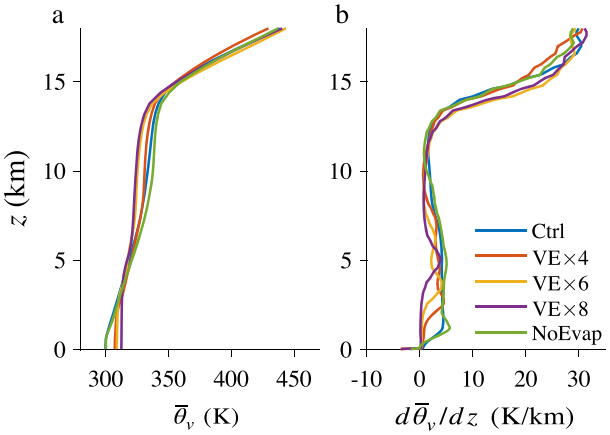

Figure B1. Vertical profiles for domain-averaged (a) θ_v and (b) $d\theta_v/dz$ in five aggregated simulations: control simulation (Figure 1a); 4, 6, and 8 times virtual effect (VE) simulation (the last three panels of the first row in Figure 5); and no-evaporation simulation (Figure 7d). The control and no-evaporation profiles are similar, but the profiles in the virtual effect simulation deviates. This is likely due to enhanced surface buoyancy flux deepening the boundary layer.

We use scale analysis to show that individual cold pools cannot inhibit convective self-aggregation due to a separation of the two spatial scales. We further suggest that evaporative cooling inhibits self-aggregation by reducing APE. This analysis, however, does not rule out possible effects due to the aggregated effect of multiple cold pools. For example, if there are about 50 cold pools simultaneously per aggregate, they together may homogenize BL properties across moist and dry patches and thereby inhibit self-aggregation. A detailed study of cold pools in aggregation simulations will help test whether cold pools or evaporative cooling inhibits self-aggregation.

One important assumption in our framework is WBG above the BL. This assumption holds in slowly rotating atmospheres, for example, the tropical atmosphere. The theoretical framework may, therefore, have implications on tropical circulations, such as the MJO. It would be worth to examine if the MJO have similar sensitivities to BL radiative cooling, surface fluxes, the virtual effect, and evaporation of raindrops.

Do FT processes matter? The answer is yes, and let us take radiation as an example. Radiation leads to convective aggregation by cooling the high-pressure area in the BL. However, radiation is a nonlocal process, and the efficient BL cooling results from a dry FT. A more complete understanding may require coupling the BL and FT together.

Appendix A: APE Production Due to Surface Fluxes

In equation (4), the buoyancy source $S_b = -\partial_z F$, where F is the diabatic flux associated with a particular process. The APE production (APEP) is then given by

$$APEP = \frac{1}{L}\int_0^L dx \int_0^z dz' \frac{\rho_0 \tilde{b}}{N^2}(-\tilde{\partial}_z F). \tag{A1}$$

Integration by parts gives

$$APEP = -\frac{1}{L}\int_0^L dx \int_0^z dz' \partial_z \left(\frac{\rho_0 \tilde{b}}{N^2}\tilde{F}\right) + \frac{1}{L}\int_0^L dx \int_0^z dz' \tilde{F}\partial_z \left(\frac{\rho_0 \tilde{b}}{N^2}\right). \tag{A2}$$

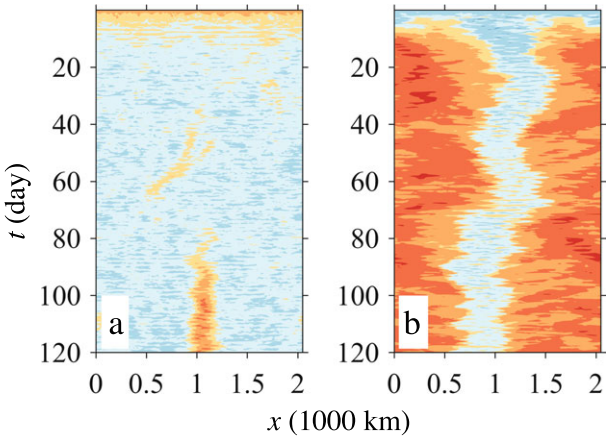

Figure B2. Hovmoller diagrams of precipitable water (mm). (a) A simulation with horizontally homogenized radiative cooling for the lowest 1 km. Weak convective self-aggregation starts to develop around day 80, suggesting enough APE could be generated above 1 km. (b) A simulation with 8× virtual effect starting from its corresponding radiative-convective equilibrium profile. The results are qualitative similar to the up right corner in Figure 5.

Here we focus on the surface flux contribution to APEP, so $F = F_S$, which is 0 outside an infinitesimal layer at surface. The second term of the right-hand side then goes to 0. The APEP due to surface fluxes is

$$APEP = \frac{1}{L}\int_0^L dx \left(\frac{\rho_0 \tilde{b}}{N^2}\bigg|_{z=0} \tilde{F}_S\right) = \left(\rho_0 \frac{\overline{\tilde{b}\tilde{F}_S}}{N^2}\right)\bigg|_{z=0}. \tag{A3}$$

We then use (A3) to diagnose APEP due to surface buoyancy fluxes in our simulations.

Appendix B: Mean States and Sensitivity Experiments

We show domain-averaged profiles of aggregated simulations (Figure B1), sensitivity experiments with different BL tops (Figure B2a) and different initial sounding profiles (Figure B2b), and an experiment without nudging horizontal winds (Figure B3). The color schemes are the same as in the main text.

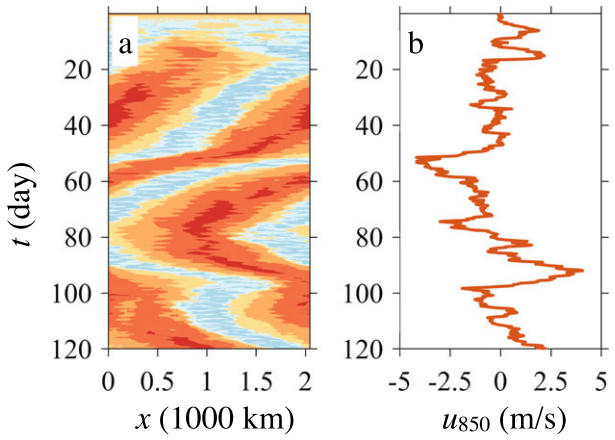

Figure B3. Testing if nudging horizontal winds affects the proposed surface flux feedback in the 6× virtual effect simulation (the third panel of the first row in Figure 5). (a) Hovmoller diagram for precipitable water (mm), and (b) horizontally averaged wind at 850 hPa. The drift of the large-scale moisture anomaly may be associated with horizontal advection by winds.

Acknowledgments
This work was supported by Laboratory Directed Research and Development (LDRD) funding from Berkeley Lab, provided by the Director, Office of Science, of the U.S. Department of Energy under contract DE-AC02-05CH11231. The author was also supported by a Miller Research Fellowship at the University of California, Berkeley. The author would like to thank N. Brenowitz, C. Bretherton, D. Romps, Adam Sobel, and Z. Tan for helpful discussions. Comments and suggestions from Z. Kuang and anonymous reviewers helped improve the manuscript substantially. The numerical model was developed by M. Khairoutdinov and can be obtained at http://rossby.msrc.sunysb.edu/~marat/SAM.html. All input files for the numerical simulations are available upon requests.

References

Abbot, D. S. (2014). Resolved snowball Earth clouds. *Journal of Climate*, *27*(12), 4391–4402. https://doi.org/10.1175/JCLI-D-13-00738.1

Arnold, N. P., & Randall, D. A. (2015). Global-scale convective aggregation: Implications for the Madden-Julian Oscillation. *Journal of Advances in Modeling Earth Systems*, *7*, 1499–1518. https://doi.org/10.1002/2015MS000498

Bretherton, C. S., Blossey, P. N., & Khairoutdinov, M. (2005). An energy-balance analysis of deep convective self-aggregation above uniform SST. *Journal of the Atmospheric Sciences*, *62*(12), 4273–4292. https://doi.org/10.1175/JAS3614.1

Charney, J. G. (1963). A note on large-scale motions in the tropics. *Journal of the Atmospheric Sciences*, *20*(6), 607–609. https://doi.org/10.1175/1520-0469(1963)020<0607:ANOLSM>2.0.CO;2

Charney, J. G., & Eliassen, A. (1964). On the growth of the hurricane depression. *Journal of the Atmospheric Sciences*, *21*(1), 68–75. https://doi.org/10.1175/1520-0469(1964)021<0068:OTGOTH>2.0.CO;2

Collins, W. D., Rasch, P. J., Boville, B. A., Hack, J. J., McCaa, J. R., Williamson, D. L., et al. (2006). The formulation and atmospheric simulation of the community atmosphere model version 3 (CAM3). *Journal of Climate*, *19*(11), 2144–2161. https://doi.org/10.1175/JCLI3760.1

Coppin, D., & Bony, S. (2015). Physical mechanisms controlling the initiation of convective self-aggregation in a General Circulation Model. *Journal of Advances in Modeling Earth Systems*, *7*, 2060–2078. https://doi.org/10.1002/2015MS000571

Cronin, T. W. (2014). On the choice of average solar zenith angle. *Journal of the Atmospheric Sciences*, *71*(8), 2994–3003. https://doi.org/10.1175/JAS-D-13-0392.1

Emanuel, K. A., David Neelin, J., & Bretherton, C. S. (1994). On large-scale circulations in convecting atmospheres. *Quarterly Journal of the Royal Meteorological Society*, *120*(519), 1111–1143. https://doi.org/10.1002/qj.49712051902

Emanuel, K., Wing, A. A., & Vincent, E. M. (2014). Radiative-convective instability. *Journal of Advances in Modeling Earth Systems*, *6*, 75–90. https://doi.org/10.1002/2013MS000270

Garratt, J.-R. (1994). Review: The atmospheric boundary layer. *Earth-Science Reviews*, *37*(1–2), 89–134. https://doi.org/10.1016/0012-8252(94)90026-4

Gentine, P., Garelli, A., Park, S.-B., Nie, J., Torri, G., & Kuang, Z. (2016). Role of surface heat fluxes underneath cold pools. *Geophysical Research Letters*, *43*, 874–883. https://doi.org/10.1002/2015GL067262

Held, I. M., Hemler, R. S., Ramaswamy, V., Held, I. M., Hemler, R. S., & Ramaswamy, V. (1993). Radiative-convective equilibrium with explicit two-dimensional moist convection. *Journal of the Atmospheric Sciences*, *50*(23), 3909–3927. https://doi.org/10.1175/1520-0469(1993)050<3909:RCEWET>2.0.CO;2

Holloway, C. E., & Woolnough, S. J. (2016). The sensitivity of convective aggregation to diabatic processes in idealized radiative-convective equilibrium simulations. *Journal of Advances in Modeling Earth Systems*, *8*, 166–195. https://doi.org/10.1002/2015MS000511

Jeevanjee, N., & Romps, D. M. (2013). Convective self-aggregation, cold pools, and domain size. *Geophysical Research Letters*, *40*, 994–998. https://doi.org/10.1002/grl.50204

Khairoutdinov, M. F., & Randall, D. A. (2003). Cloud resolving modeling of the ARM summer 1997 IOP: Model formulation, results, uncertainties, and sensitivities. *Journal of the Atmospheric Sciences*, *60*(4), 607–625. https://doi.org/10.1175/1520-0469(2003)060<0607:CRMOTA>2.0.CO;2

Kuang, Z. (2008a). Modeling the interaction between cumulus convection and linear gravity waves using a limited-domain cloud system—Resolving model. *Journal of the Atmospheric Sciences*, *65*(2), 576–591. https://doi.org/10.1175/2007JAS2399.1

Kuang, Z. (2008b). A moisture-stratiform instability for convectively coupled waves. *Journal of the Atmospheric Sciences*, *65*(3), 834–854. https://doi.org/10.1175/2007JAS2444.1

Muller, C., & Bony, S. (2015). What favors convective aggregation and why? *Geophysical Research Letters*, *42*, 5626–5634. https://doi.org/10.1002/2015GL064260

Muller, C. J., & Held, I. M. (2012). Detailed investigation of the self-aggregation of convection in cloud-resolving simulations. *Journal of the Atmospheric Sciences*, *69*(8), 2551–2565. https://doi.org/10.1175/JAS-D-11-0257.1

Naumann, A. K., Stevens, B., Hohenegger, C., & Mellado, J. P. (2017). A conceptual model of a shallow circulation induced by prescribed low-level radiative cooling. *Journal of the Atmospheric Sciences*, *74*(10). JAS–D–17–0030.1, https://doi.org/10.1175/JAS-D-17-0030.1

Pritchard, M. S., & Yang, D. (2016). Response of the superparameterized Madden-Julian Oscillation to extreme climate and basic state variation challenges a moisture mode view. *Journal of Climate*, *29*, 4995–5008. JCLI–D–15–0790.1, https://doi.org/10.1175/JCLI-D-15-0790.1

Sobel, A. H., Nilsson, J., & Polvani, L. M. (2001). The weak temperature gradient approximation and balanced tropical moisture waves*. *Journal of the Atmospheric Sciences*, *58*(23), 3650–3665. https://doi.org/10.1175/1520-0469(2001)058<3650:TWTGAA>2.0.CO;2

Tompkins, A. M. (2001). Organization of tropical convection in low vertical wind shears: The role of water vapor. *Journal of the Atmospheric Sciences*, *58*(6), 529–545. https://doi.org/10.1175/1520-0469(2001)058<0529:OOTCIL>2.0.CO;2

Tompkins, A. M., & Semie, A. G. (2017). Organization of tropical convection in low vertical wind shears: Role of updraft entrainment. *Journal of Advances in Modeling Earth Systems*, *9* 1046–1068. https://doi.org/10.1002/2016MS000802

Vallis, G. (2017). *Atmospheric and oceanic fluid dynamics: Fundamentals and large-scale circulation*. Cambridge: Cambridge University Press. https://doi.org/10.1017/9781107588417

Wing, A. A., & Cronin, T. W. (2015). Self-aggregation of convection in long channel geometry. *Quarterly Journal of the Royal Meteorological Society*, *142*(694), 1–15. https://doi.org/10.1002/qj.2628

Wu, Z. (2003). A shallow CISK, deep equilibrium mechanism for the interaction between large-scale convection and large-scale circulations in the tropics. *Journal of the Atmospheric Sciences*, *60*, 377–392. https://doi.org/10.1175/1520-0469(2003)060<0377:ASCDEM>2.0.CO;2

Yang, D. (2018). Boundary layer height and buoyancy determine the horizontal scale of convective self-aggregation. *Journal of the Atmospheric Sciences*, *75*, 469–478. JAS–D–17–0150.1, https://doi.org/10.1175/JAS-D-17-0150.1

Yang, D., & Ingersoll, A. P. (2013). Triggered convection, gravity waves, and the MJO: A shallow-water model. *Journal of the Atmospheric Sciences*, *70*(8), 2476–2486. https://doi.org/10.1175/JAS-D-12-0255.1

Yang, D., & Ingersoll, A. P. (2014). A theory of the MJO horizontal scale. *Geophysical Research Letters*, *41*, 1059–1064. https://doi.org/10.1002/2013GL058542